

## Research Paper

# Large-scale shallow foundation load tests on soft clay – At the National Field Testing Facility (NFTF), Ballina, NSW, Australia



F.M. Gaone<sup>a,\*</sup>, S. Gourvenec<sup>a</sup>, J.P. Doherty<sup>b</sup>

<sup>a</sup> Centre for Offshore Foundation Systems, University of Western Australia, Perth, Western Australia, Australia

<sup>b</sup> School of Civil, Environmental and Mining Engineering, University of Western Australia, Perth, Western Australia, Australia

## ARTICLE INFO

## Keywords:

Shallow foundations  
Field testing  
Soft clay

## ABSTRACT

This paper presents field test data from four instrumented rigid square pad foundations on soft clay that were brought to failure under concentric vertical loading. The test programme comprised two unconsolidated undrained (UU) foundation tests as well as two consolidated undrained (CU) tests. In the latter case the two foundations were preloaded to a proportion of the UU capacity and the soil was allowed to consolidate before being brought to undrained failure. In this paper, the site works and testing procedures are presented along with the load- and time-settlement responses of all four foundations. Horizontal stress and pore pressure data are presented for the two CU tests. The undrained and consolidated undrained load-settlement responses are shown to agree well with theoretical and numerical predictions. Results from the UU tests were the subject of a prediction exercise, summarised in a companion paper presented in this special issue.

© 2017 Elsevier Ltd. All rights reserved.

## 1. Introduction

This paper presents the results of four large-scale shallow foundation tests on soft estuarine clay carried out at the Australian National Field Testing Facility (NFTF), near Ballina, NSW, established as part of the activities of the Centre of Excellence for Geotechnical Science and Engineering (CGSE). Two rigid square pad foundations were loaded concentrically to failure in an unconsolidated and undrained condition (UU1 and UU2). Another two foundations were loaded with 30% and 50% of the measured UU failure load and allowed to fully consolidate before being brought to failure under undrained vertical concentric loads (CU1 and CU2). In this paper, the foundation response is analysed in conjunction with high quality site investigation data. An international shallow foundation prediction exercise was run in conjunction with these field tests to assess the current state of practice for predicting the undrained load-settlement response and ultimate capacity of shallow foundations. The outcomes of the prediction exercise are presented in a companion paper in this special issue [1].

Results of large-scale foundation tests on soft clay under vertical centric loading are sparse in the literature, and most notably include those carried out at the UK's national soft soil test site, in

Bothkennar, Scotland [2,3]. The Bothkennar site was extensively characterised as part of the research initiative [4]. The philosophy of the NFTF, at which the tests presented in this paper were carried out, was based on the Bothkennar exemplar. Similarities also exist in terms of the site conditions and foundation geometry. The Bothkennar site comprised a weathered crust to around 2 m depth below ground level overlying clay and silt that were deposited under marine or estuarine conditions with the summer water table 0.9 m below ground level [2]. The undrained shear strength within the clay/silt layer was also similar at the two sites. At Bothkennar, five rigid square pad foundations, of the same shape and similar size were tested over a period of 11 years enabling insights into the effect of long term preloading on foundation bearing capacity. However, some notable differences preclude direct comparison of outcomes from the Bothkennar tests and those from the NFTF. For example, the Bothkennar foundations are cast within the crust layer rather than at the top of the underlying estuarine clay layer as at the NFTF and the rate of loading to failure of the foundations at Bothkennar was two orders of magnitude slower than those at the NFTF, while the consolidation period between sets of tests was an order of magnitude greater. The experimental approach adopted for the Bothkennar field tests was drawn from earlier work of field tests on clays [5–9].

The shallow foundation construction details and observed performance, as presented in this paper, are freely available in digital form through [www.geocalcs.com/datamap](http://www.geocalcs.com/datamap) [10]. The site data and

\* Corresponding author.

E-mail address: [21445055@student.uwa.edu.au](mailto:21445055@student.uwa.edu.au) (F.M. Gaone).

results from all the laboratory and in situ testing are also available through the online platform.

## 2. Site, ground conditions and foundation description

### 2.1. The site

The NFTF is located in the north western part of Ballina, NSW on the east coast of Australia, (see Fig. 1). The site is approximately 6.5 Ha in area and is bounded by creeks to the north and east and sugar cane fields along the other boundaries (see Fig. 2). Prior to the CGSE leasing the site in 2013, the area was used to farm sugar cane. The sugar cane was cleared and a site road was constructed to enable access for various research activities, which included the large-scale shallow foundation tests reported in this paper, large-scale embankment testing [11], and a range of in situ geotechnical testing and sampling for laboratory testing [12–17]. An aerial view indicating the location of the various activities is shown in Fig. 3.

### 2.2. Ground conditions

The site comprises a crust layer of alluvial clayey silty sand to a depth of about 1.5 m, underlain by soft estuarine clay with a thickness varying between 12 m and 22 m. From the observation of boreholes (drilled for self-boring pressuremeter tests) close to the position of the foundation tests, the natural groundwater level was observed to be at  $\sim 1.0$  m depth ( $-0.5$  m AHD), in March 2014. Laboratory and in-situ testing from the site are described in the literature [12,13,15–17]. Data from these publications has been made available in a free-to-access web application [www.geocalcs.com/datamap](http://www.geocalcs.com/datamap) [10].

Fig. 4 illustrates the stratigraphy and key material properties from the site investigation data at the shallow foundation test site. Unit weights were determined from laboratory tests; undrained shear strength profiles were obtained from self-boring pressuremeter (SBPM), piezocone (CPTu) and triaxial compression tests (TXC); shear modulus from TXC and SBPM tests; permeability and coefficient of vertical and horizontal consolidation from constant rate of strain (CRS), incremental load (IL), in situ ball penetrometer and CPTu tests.

The secant shear modulus of the triaxial data,  $G_{10}$  and  $G_{50}$  were interpreted using two different points on the curve of the total change in deviatoric stress (10% and 50% of the total change in deviatoric stress). Interpretation of the shear modulus from SBPM tests was performed using an inverse analysis ( $G_{IA}$ ) method [18] and from the slope of unload-reload loops ( $G_{UR}$ ).

### 2.3. Foundations and loading blocks

Four square foundations with 1.8 m edge lengths and 0.6 m thick were cast 1.5 m below ground level, at the top of the estuarine clay layer, in June 2014. The construction procedure for each foundation was identical. The geometry and configuration of the foundations is illustrated in Fig. 5. A square foundation pit approximately 2.4 m in edge length was excavated for construction of the foundations and due to the shear strength to stress ratio of the crust, it was possible to construct the trench with free standing vertical walls (Fig. 6). After the excavation, the foundations were cast in situ using 32 MPa concrete and timber formwork designed to withstand the concrete pressure (Fig. 7).

Reinforced concrete loading blocks were cast on-site at the same time as the foundations (Fig. 8). The blocks were constructed with the same plan dimensions as the foundations but with a height of 0.425 m, such that each block led to an increase in foundation bearing pressure of around 10 kPa. Each loading block was

cast with longitudinal tensile and vertical shear reinforcement and four lifting eyes to facilitate placement by the crane. Eight concrete blocks were constructed, as this was forecast as an upper limit to the required load to fail the foundations. During the loading procedure, each concrete block was weighed using the scale on the 35 tonne crane (the accuracy of the load cell was  $\pm 100$  kg) and the average weight was 3.3 tonnes, equivalent to a unit weight of  $24 \text{ kN/m}^3$ . Constructing the bespoke blocks to the same plan dimensions as the foundations minimized the opportunity for eccentric loading of the foundation during the test.

### 2.4. Instrumentation

All foundations were equipped with survey targets to monitor displacements during loading and consolidation stages (if included). Reflective targets were mounted on three steel reinforcement bars and attached to the first loading block, as there was insufficient space to mount them directly on the foundation. The steel bars were installed to a height sufficient to be visible above the excavation. Three targets were selected to ensure that three dimensional movements of the foundation could be captured. A licensed surveyor used a total station theodolite (TST) to measure foundation displacements. The instrument error of the TST used was given as 3 arc-second, resulting in an accuracy of 0.5 mm for the distances measured. The survey target set up is shown in Fig. 9 and is also visible in Fig. 13.

For the CU tests, three Vibrating Wire Push-in Pressure Cells [19] (also known as spade cells based on their shape) were installed beneath each foundation at depths of 0.6 m, 1.3 m and 2.0 m to measure changes in total horizontal stress and pore water pressure during loading and consolidation. The pressure cells were offset from the centre of the foundation by 0.6 m. The layout of the ground instrumentation is illustrated in Figs. 10 and 11.

## 3. Test programme and procedures

### 3.1. Test programme

The entire programme ran from June 2014 to March 2016. The timeline illustrating the key stages is shown in Fig. 12 and three main stages are described below

Stage 1: Site works for the shallow foundation field tests commenced in June 2014, involving site clearance; excavation of the foundation pit through the surficial crust layer to the top of the soft estuarine clay (Fig. 6); dewatering of the excavation; and construction of the formwork and casting of the foundation in situ in the excavated pit (Fig. 7).

Stage 2: The second stage of site activities commenced in September 2014 and involved dewatering the excavated pit, removing the formwork and undrained loading of two foundations to failure (UU1 and UU2). Following the UU tests, the remaining two foundations were loaded to 30% and 50% of the failure load obtained from the undrained tests in preparation for the consolidated undrained foundation tests, CU1 and CU2. The load was maintained constant for a period of 18 months to allow consolidation. The settlements during the consolidation process were recorded by a licensed surveyor in increasing time increments until no further movement was observed in May 2015 (see surveying points in Fig. 12).

Stage 3: The third stage of site activity commenced in March 2016 and involved the application of a further load increment to each foundation, followed by a consolidation period of 6 days and final undrained loading of the foundations to failure (CU1 and CU2).



Fig. 1. Location of the National Field Testing Facility (NFTF) at Ballina, New South Wales, Australia.



Fig. 2. Aerial view showing the location of the National Field Testing Facility (NFTF) site.

### 3.2. Testing procedures

The foundations were loaded to failure in approximately 1 tonne increments over a time scale to ensure an undrained soil response. The 35 tonne crane placed the pre-cast concrete blocks one at a time, releasing the load in increments of approximately 1 tonne. Fig. 13 shows the general loading procedure. Survey measurements of the three corner targets were taken after each load increment was applied. The average time for one load increment was 2–3 min. The time between the load increments increased to

approximately 5 min when a new block was placed as it took a several minutes to unhook the loading eyes of the previous block and hook the next block. The pause between the load increments was increased as the foundation approached failure to allow for at least two sets of recordings by the surveyor. The loading sequences took between 30 and 70 min. The loading time histories for the two UU tests are shown in Fig. 14. The same procedure was adopted for the undrained loading to failure stage of the preloaded foundation tests (CU).

Prior to loading to failure, each CU test comprised two load and two consolidation stages, illustrated in Fig. 15. The preload

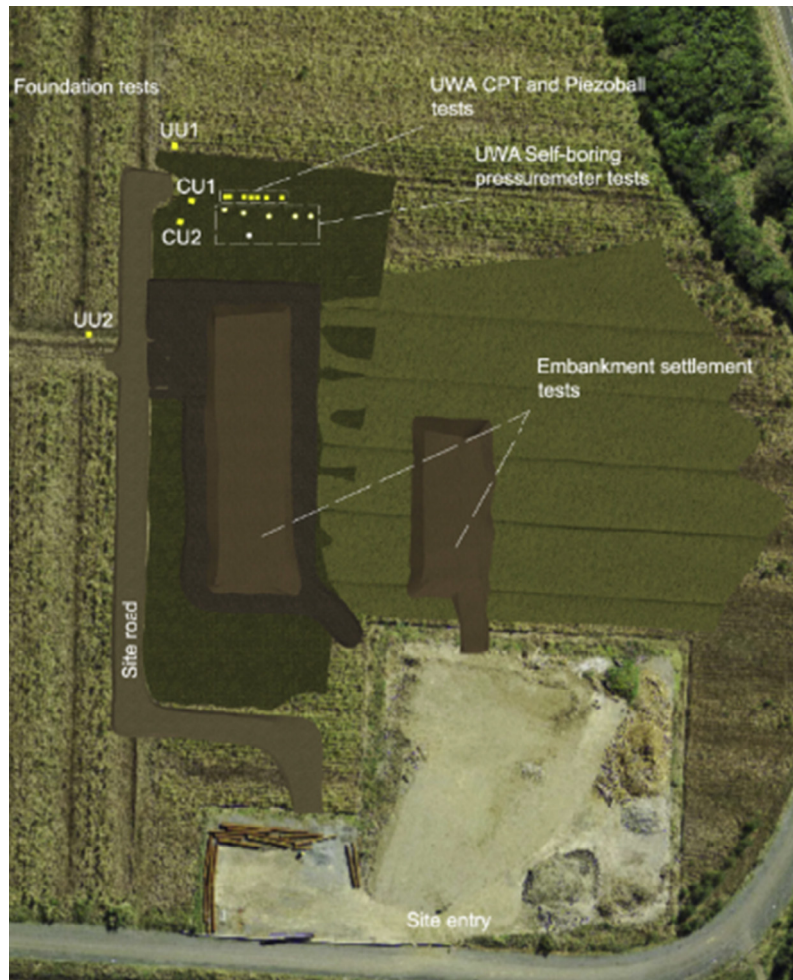


Fig. 3. Plan showing locations of in situ tests, instrumented embankments and shallow foundations at the National Field Testing Facility (NFTF).

is described as a proportion of the bearing capacity observed in the UU tests ( $V_p/V_{UU}$ ), where the load  $V$  is given by the product of the bearing pressure and plan area of the foundation,  $qA$ . In the first load stage, the foundations were loaded to  $V_p/V_{UU} = 0.33$  and  $0.50$ , corresponding to  $20$  kPa for CU1 and  $30$  kPa for CU2 (2 blocks for CU1 and 3 blocks for CU2). The initial loading step was followed by a consolidation period of approximately 18 months (540 days). An additional preloading stage was subsequently carried out to assist in clarifying an uncertainty in the interpretation of the recorded stresses from the spade cells (further discussed in the results section). An additional two loading blocks were added to each foundation raising the relative preload  $V_p/V_{UU}$  to  $0.67$  and  $0.83$ , corresponding to  $40$  kPa for CU1 and  $50$  kPa for CU2. The second loading stage was followed by a second consolidation stage of 6 days. The final undrained loading to failure of the CU tests used the procedure described above.

Due to the higher than planned preload, failure of the foundation for test CU1 required all eight concrete loading blocks to be used. This required CU2 to be unloaded prior to its final loading stage (see Final loading stage in Fig. 15). The total time between the complete unloading of CU2 and the final loading was less than 20 min. Complications during reloading CU2 required the loading blocks to be stacked with a slight eccentricity, 5–10 cm, to avoid damaging of the surveying targets. The possible effect of the eccentricity is discussed later with the presentation of the load-settlement response.

## 4. Results & interpretation

### 4.1. Unconsolidated undrained foundation tests (UU)

#### 4.1.1. Observed response

The load-settlement behaviour of test UU1 and UU2, taken from the crane load and survey measurements, are shown in Fig. 16. It can be seen, that the three corner targets of both foundations settled uniformly and approximately linearly to a bearing pressure of  $50$  kPa. Beyond  $50$  kPa, the load-settlement response became non-uniform and non-linear and the foundations started to tilt, indicated by the settlement reading of corner target B decreasing while the settlements of targets A and C continued increasing. The failure modes observed in test UU1 and UU2 are shown in Fig. 17.

Bearing capacity was defined at the point at which the foundation movements increased without any change in load, identified from the time dependent settlements ( $\Delta s/\Delta t$ ) between loading steps, i.e. at constant load (Fig. 18). At an applied pressure of  $60$  kPa, the rate of settlement in tests UU1 and UU2 started to increase rapidly, and is thus taken as the bearing capacity.

#### 4.1.2. Interpretation of undrained load-settlement response and bearing capacity

The excavation in which the foundation was cast and the gap between the foundation and excavation walls complicates the boundary conditions, such that simple hand calculations are not

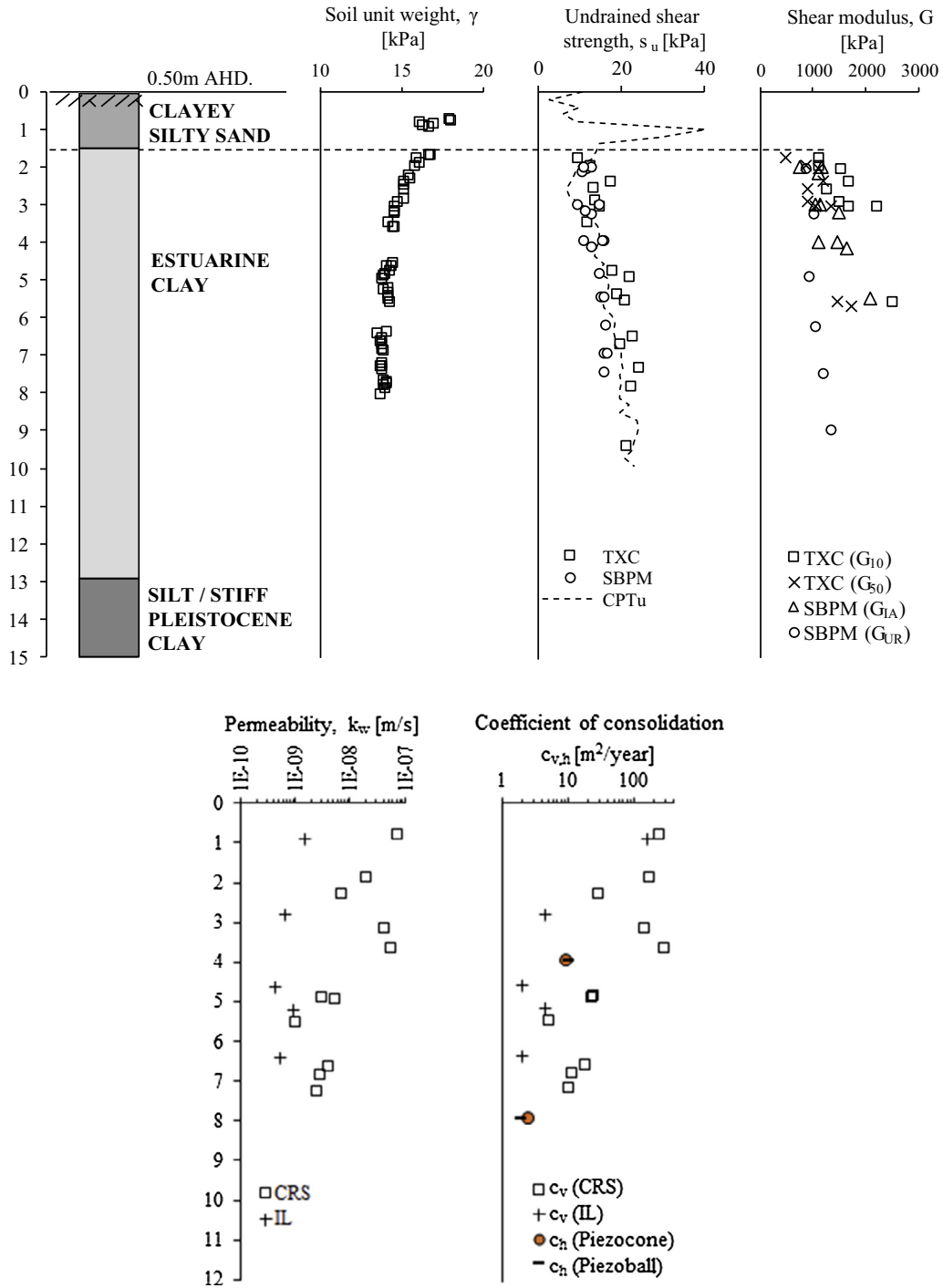


Fig. 4. Stratigraphy and soil profile at the test site.

well suited to the interpretation and a finite element approach in which the geometry could be represented was adopted.

An axisymmetric model using the Abaqus finite element software package was created. The finite element model, shown in Fig. 19 was created using 4840, 8-noded quadratic elements (reduced integration). The geometry of the excavation, gap and foundation were modelled as outlined in Fig. 11 and the foundation was loaded in the same increments of load as on site. The square foundation geometry and excavation were idealised as circular with equivalent respective areas. The two different soil layers were modelled to represent the crust and the underlying soft clay.

The model was sufficiently large to avoid disturbances by the fixed base and side boundaries.

The crust was modelled as an elastic perfectly plastic material with Young's modulus  $E = 3 \text{ MPa}$  and undrained shear strength  $s_u = 25 \text{ kPa}$  based on interpretations of CPT test results [13] and Fig. 4. A parametric study was carried out varying the crust properties, which were found to have no influence on the observed foundation or soil response.

For the soft clay layer, a linear elastic perfectly plastic Tresca model was adopted. The shear modulus and undrained shear strength profiles were based on the data in Fig. 4. In the soft clay,

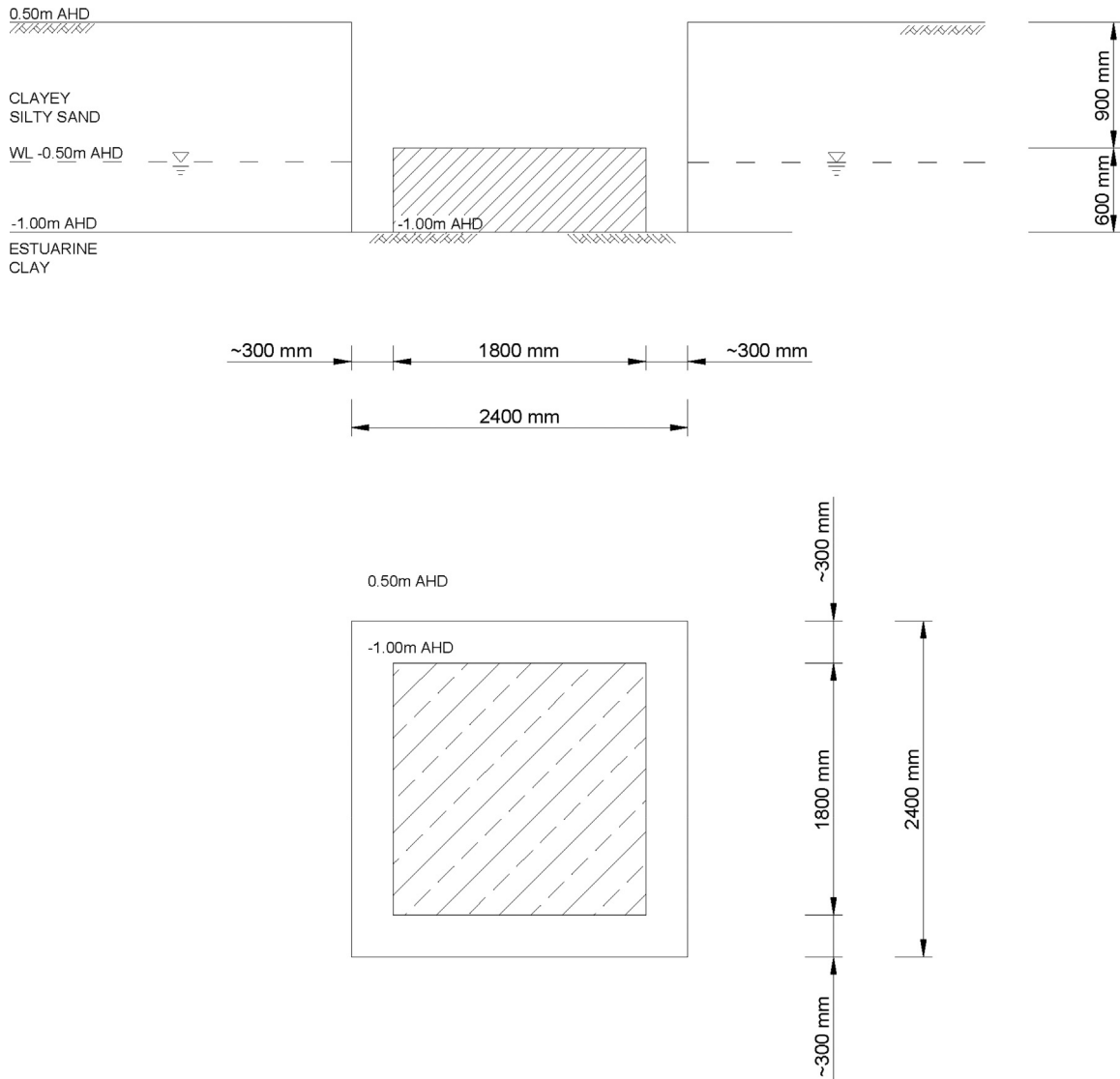


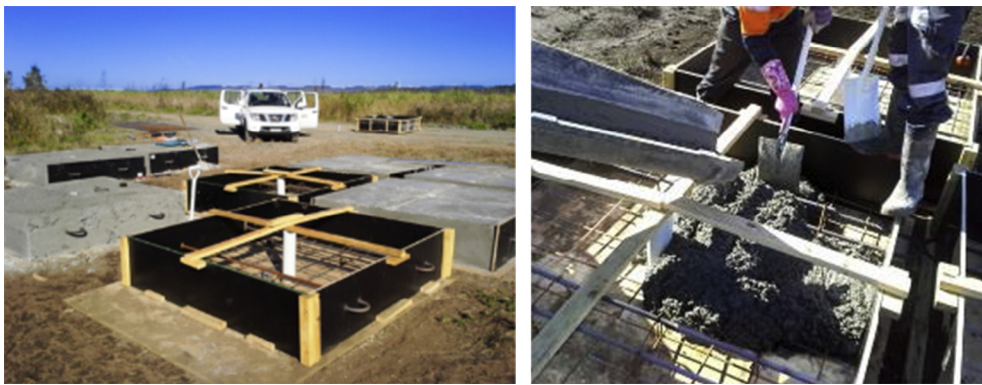
Fig. 5. Geometry and configuration of shallow foundation tests.



Fig. 6. Foundation excavation indicating free-standing vertical trench walls.



**Fig. 7.** Foundation construction (left) Pouring concrete into foundation formwork around instrumentation tubes (right) completed foundation after casting.



**Fig. 8.** Loading block construction (left) construction of timber formwork for the loading blocks and cast loading blocks and (right) pouring concrete into reinforcement cage for loading blocks.



**Fig. 9.** Survey target set up for monitoring foundation displacements.

the  $G_{50}$  and  $G_{10}$  profiles from triaxial compression tests (TXC) give lower and upper bounds to the shear modulus data while the self-boring pressuremeter (SBPM) data gives an intermediate profile. The best estimate shear modulus profile in the soft clay was idealised using a power law variation with depth ( $z$ ) described by

$$G(z) = G_R \left( \frac{z}{R} \right)^\alpha \quad (1)$$

where  $G(z)$  is the shear modulus at a depth  $z$ ,  $G_R$  is the shear modulus at a depth equal to the radius of the foundation  $R$ , and  $\alpha$  is the heterogeneity parameter that varies between zero and one. For the simulation of the foundation settlements, the shear modulus profile was fitted to the SBPM data shown in Fig. 4. The best fit was

achieved taking  $G_R = 700$  kPa and  $\alpha = 0.7$  and the resulting shear modulus profile was adopted for the FEA. A Poisson's ratio  $\nu = 0.495$  was adopted to reflect the incompressible nature of the undrained response but avoid numerical difficulties with using 0.5. The best estimate undrained shear strength profile in the soft clay was based on the profile interpreted from the SBPM data and can be approximated as linearly increasing with depth by  $s_u$  (kPa) =  $10 + 1.3(z - z_{fdn})$  where  $z$  is in m below the ground level and  $z_{fdn}$  is the depth below ground level to foundation level.

The load-settlement response predicted from the FEA is shown in Fig. 20 compared with the average observed foundation load-settlement response, taken at the centre of the foundation for each of the UU tests, and is shown to provide a reasonable estimate. The response of test UU2 is slightly stiffer and stronger than UU1, possibly due to slight variations in ground conditions (UU1 and UU2 were 60 m apart). The plastic shear strain at failure, predicted by the FEA is illustrated in Fig. 21, indicating the failure mechanism. It can be seen, that the mechanism is localised, extending only to the edge of the excavation. The localised mechanism indicates that the stronger crust layer has forced the failure mechanism to occur inside the gap between the foundation and excavation wall. It is noted that assuming the foundation is embedded with no gap, leads to considerable over-prediction of the observed capacity, whether via FEA or a simple hand calculation with a bearing capacity factor for an embedded foundation with no gap accounted for (e.g. [20,21]). The effect of the size of the gap on the magnitude of mobilised bearing capacity is further investigated in the companion paper accompanying the shallow foundation prediction exercise [1].

The discussion above has shown that the observed foundation load-settlement response and undrained bearing capacity can be

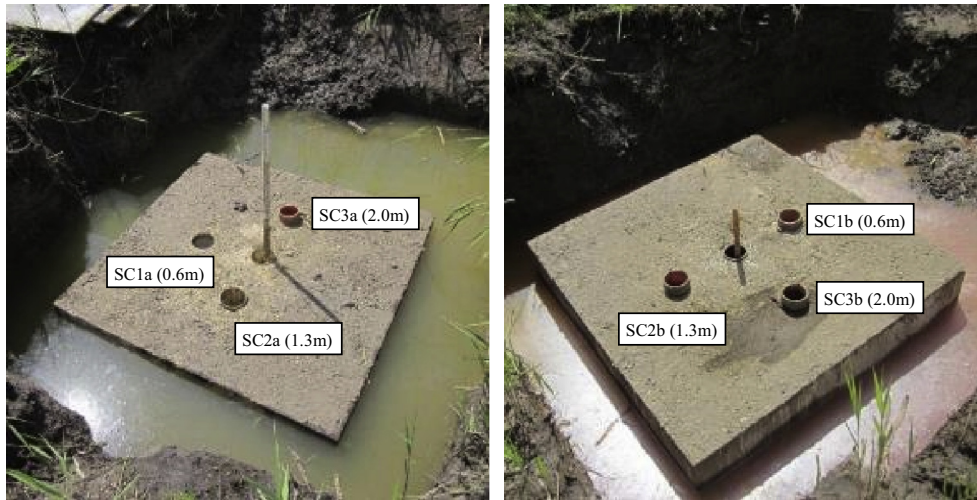
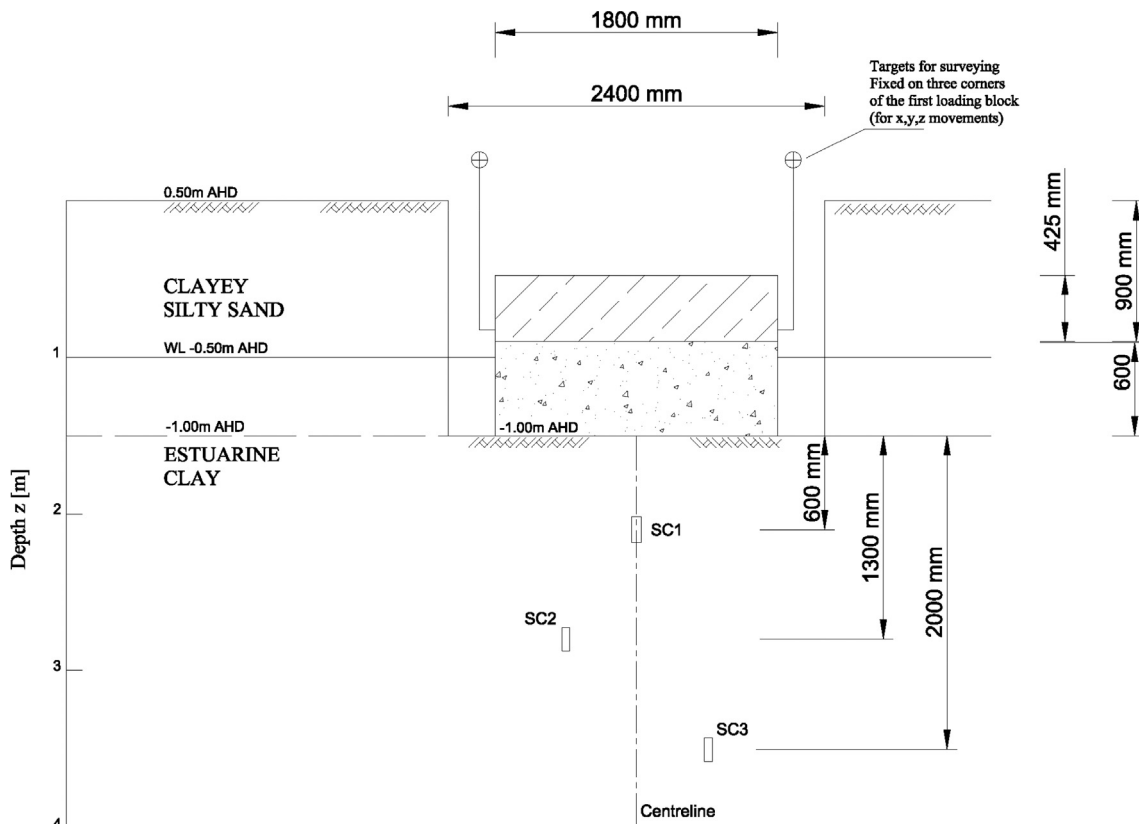


Fig. 10. Foundations cast in situ showing instrumentation for the consolidated undrained foundation tests (CU1 and CU2).



Note: SC1 is offset an equal distance out of plane as SC2 and SC3 are to the centreline shown

Fig. 11. Instrumentation layout for the consolidated undrained foundation tests (CU1 and CU2).

reasonably predicted from the available site investigation data and a simple constitutive model, provided the presence of the gap is modelled.

#### 4.2. Consolidated undrained foundation tests (CU)

##### 4.2.1. Observed response

The load-settlement and time-settlement response at each stage of the consolidated undrained foundation tests (CU1 and CU2) are shown in Figs. 22 and 23. Results are presented for the

three loading and two consolidation stages and represent the average foundation settlement, taken at the centre of the foundation. The movements of the three corner targets in both CU tests were uniform in all stages, except the latter stages of the final loading stage (as observed in the UU tests). The total horizontal stress and pore water pressure changes, captured from the three spade cells, located 0.6 m, 1.3 m and 2.0 m beneath foundation test CU2 are shown in Fig. 24. The data is separated into different time scales for the loading and consolidation stages to enable detailed observation of the soil response to external changes. The spade

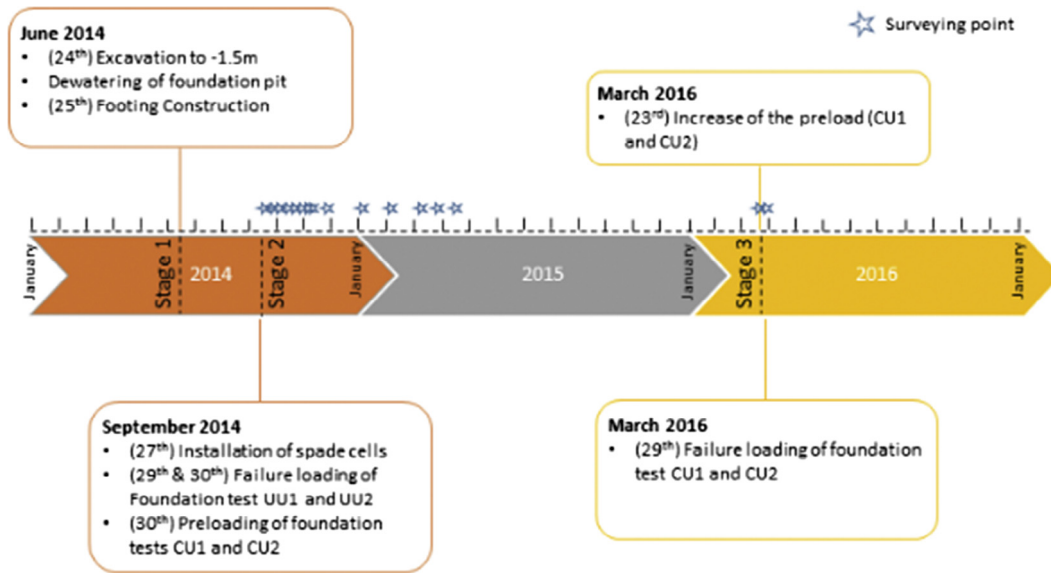


Fig. 12. Timeline of the foundation testing and surveying.



Fig. 13. Loading procedure of the unconsolidated undrained foundation tests (UU1 and UU2).

cells beneath the foundation for test CU1 malfunctioned and so stress and porewater pressure changes cannot be presented.

In the following sections, the undrained load-settlement response, consolidation response and the consolidated undrained bearing capacity are discussed.

#### 4.2.2. Interpretation of consolidated undrained load-settlement response and bearing capacity

The axisymmetric finite element mesh described above for interpreting the UU response (Fig. 19) was used but with a stress-fluid coupled critical state constitutive model for the estuarine clay. The crust was modelled as an elastic perfectly plastic material as in the analysis of the UU test. The Modified Cam Clay (MCC) model was adopted to represent the soil response of the soft clay with parameters derived through an optimization analysis of undrained self-boring pressuremeter tests [18]. The optimization method focused on matching the undrained shear strength and stress strain response from the self-boring pressuremeter and focused on matching composite parameters  $\Lambda$ , (where  $\Lambda = 1 - \kappa/\lambda$ )

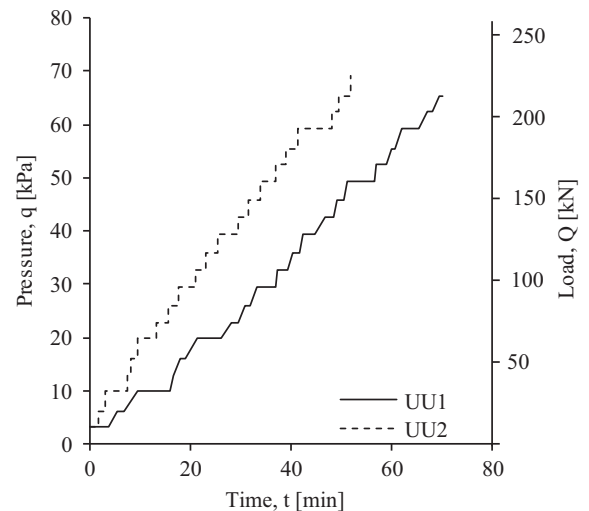


Fig. 14. Loading time history of the unconsolidated undrained (UU) foundation tests.

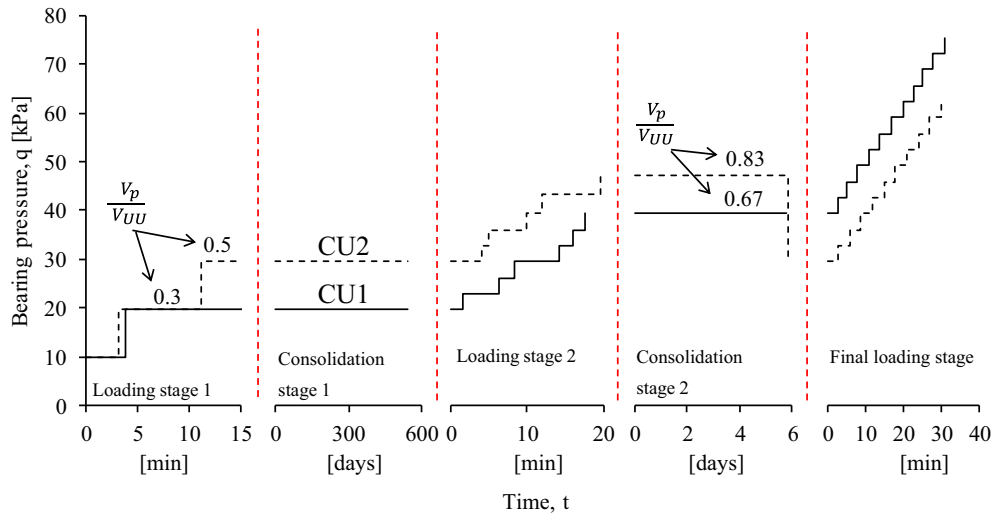


Fig. 15. Loading sequence of the consolidated undrained foundation tests (CU1 and CU2).

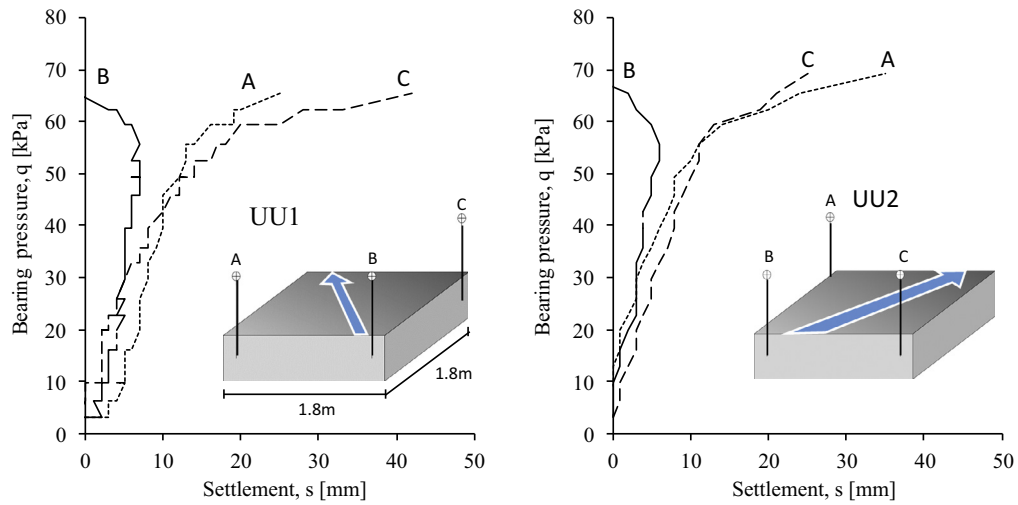


Fig. 16. Load-settlement response of the unconsolidated undrained foundation tests (UU1 and UU2).



Fig. 17. Failure modes of the unconsolidated undrained foundation tests (left: UU1 and right: UU2).

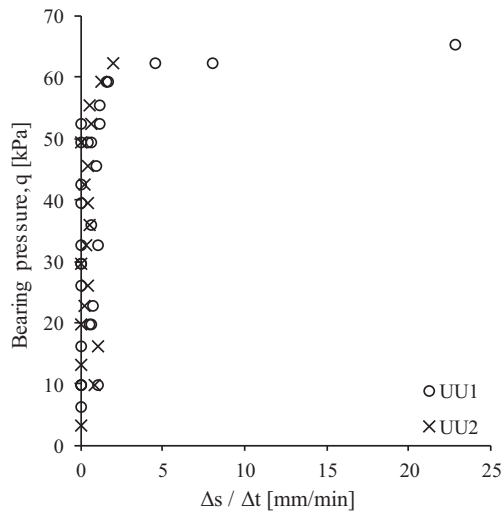


Fig. 18. Time – settlement response between loading stages of undrained unconsolidated tests UU1 and UU2.

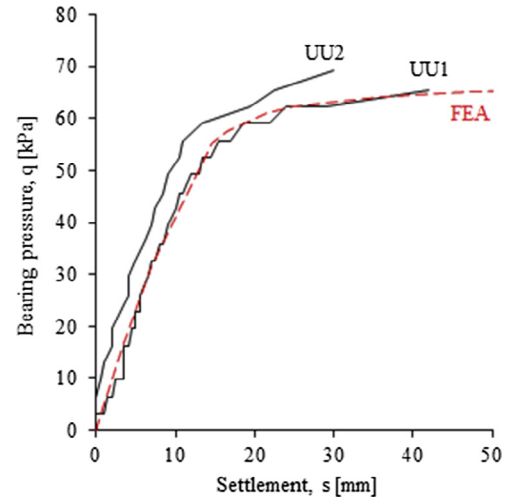


Fig. 20. Average observed load-settlement response of UU1 and UU2 compared to the results of the FEA.

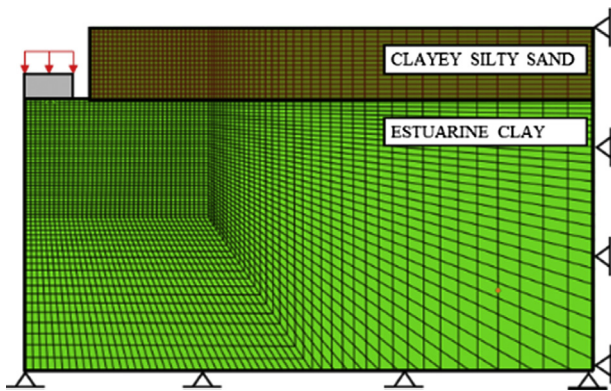


Fig. 19. FE mesh of large scale foundation tests.

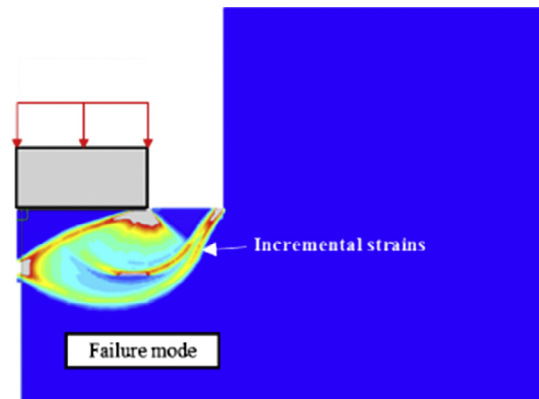


Fig. 21. Failure mechanism predicted by FEA.

$\lambda$ ) and  $\kappa^*$  (where  $\kappa^* = \kappa / (1 + e)$ , where  $\kappa$  is the slope of the unload reload line and  $\lambda$  is the slope of the normal compression line. The derived MCC parameters over depth are presented in Table 1, where  $M$  is slope of the critical state line in the  $p':q$  plane;  $R_0$  is the isotropic overconsolidation ratio; and  $\mu$  is Poisson's. Based on the information given in Fig. 4 the permeability  $k$  was taken as  $1.0E-08$  m/s and the vertical stress profile for the FEA was determined based on the soil unit weight. An average value of coefficient of earth pressure at rest,  $K_0 = 1.0$  was based on the inverse analysis of 21 SBPM tests over the depth of interest according to a numerical optimization procedure set out in the literature [18]. High-end values for  $K_0$  in sensitive clays from self-boring pressuremeter tests are not unusual and are reported in the literature [22,23]. For sensitive clays the dependence of  $K_0$  on OCR is not established [22,24,25] and does not necessarily follow the traditional expression ( $K_0 = (1 - \sin(\phi)) \text{OCR}^{\sin(\phi)}$ ) [26].  $K_0$  values for the Ballina estuarine clay are reported in the literature based on seismic dilatometer, push in pressure cells and CPT and fall in the range 0.5–1.0. The  $K_0$  values derived from the seismic dilatometer are closest to those derived from the SBPM tests, as expected.  $K_0$  values from the CPT and push in pressure cells fall in the range 0.5–1.0 and considered less reliable [27,19].

MCC parameters could alternatively be derived through a programme of element tests [13], but this does not necessarily result

in a consistent set of parameters relevant to the boundary value problem that the parameters are then applied to. The philosophy and process of the inverse analysis method for deriving an optimized and consistent set of soil parameters is discussed in detail in the literature [18].

The sequence of the key activities modelled replicated the site activities for test CU1 and included:

- Excavation of the foundation pit (undrained)
- Construction of the foundation (undrained)
- Consolidation period (30 days)
- Preloading the foundation (undrained,  $q = 20$  kPa)
- Consolidation period (540 days)
- Additional increment of preload (undrained,  $q = 40$  kPa)
- Consolidation period (6 days)
- Final undrained loading to failure (undrained)

The results of the FE simulations are compared with the observed response of test CU1 in Fig. 25 showing good agreement.

#### 4.2.3. Interpretation of undrained stiffness response

The undrained load-settlement responses during the two preloading stages and during the final undrained loading to failure of the CU tests are compared with those during the UU tests (see Fig. 26). The consolidation settlements of the CU tests are deducted to allow a direct comparison between the load-settlement

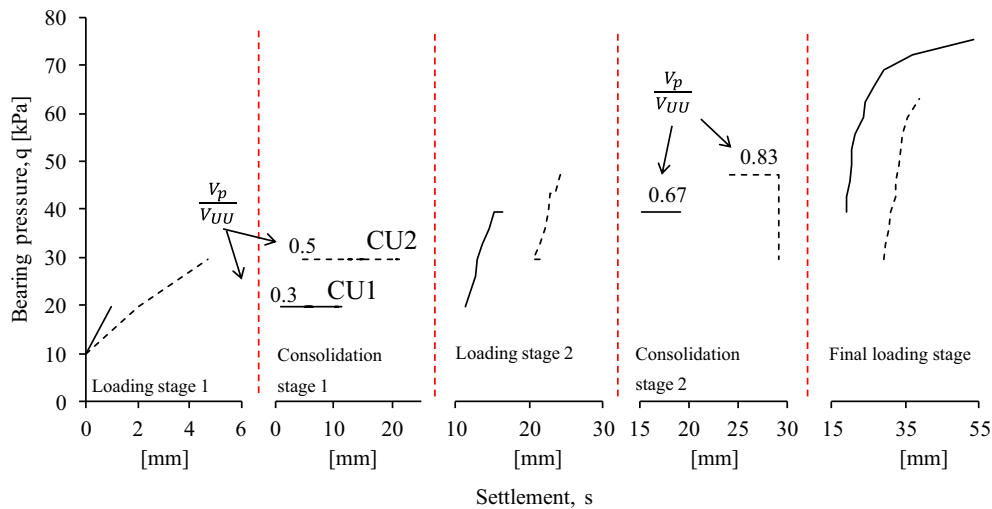


Fig. 22. Load-settlement response during the loading and consolidation stages of foundation tests CU1 and CU2.

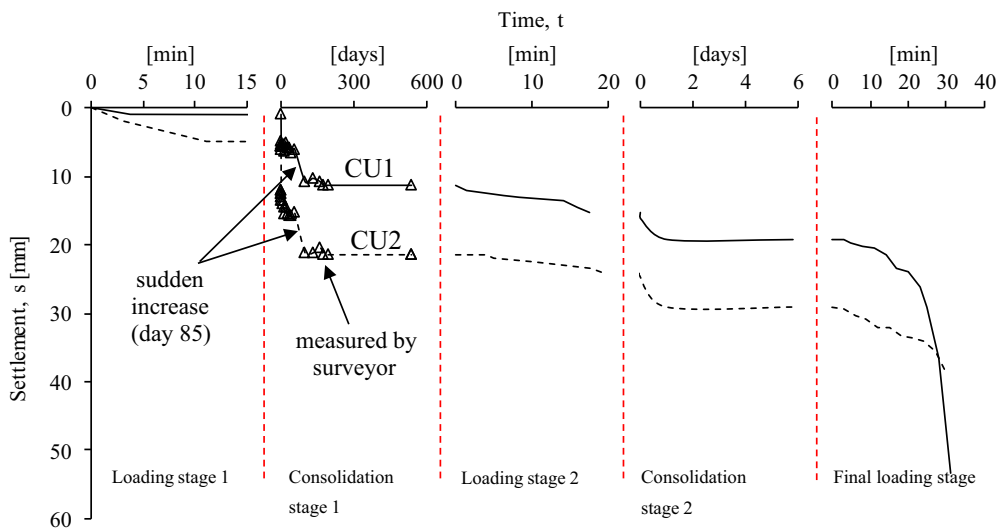


Fig. 23. Time-settlement response during the loading and consolidation stages of foundation test CU1 and CU2.

response of the undrained loading stages. The observed stiffness of CU1 was higher in each loading stage compared to CU2. The reason for this discrepancy is not immediately obvious but likely due to slight variations in soil stiffness. The increased stiffness observed in CU1 was back fitted by decreasing  $\kappa^*$  (see Fig. 25), equivalent to an increased shear modulus,  $G$ , of approximately 40%. The observed stiffness response of CU2 agrees well to that observed in both the UU tests. In general, no systematic change in stiffness was observed due to consolidation.

The pressure cell data (shown in Fig. 24) during the undrained loading events are in line with expectations, with greater soil pressure changes associated with greater preloading pressure and proximity to the ground surface. However, during the initial preloading stage, once the load was kept constant, the total stresses unexpectedly decreased, in line with the decrease in pore pressure. This behaviour was observed at each depth (albeit less significantly with increasing depth) and for both tests (CU1 and CU2). The anomalous response in total stress might be due to a redistribution of soil stress locally due to high local stresses around the spade cells generated during the installation process [28]. Retrospectively it could be surmised that a longer period for equalisation of the spade cells would have been desirable. During the

second preloading and final loading stage, the total pressure behaved as expected; i.e. remaining constant after the application of load while the recorded excess pore pressures slowly dissipated.

#### 4.2.4. Consolidation response

From Fig. 24 it can be seen that the majority of the measured excess pore pressure and associated foundation settlement, caused by the initial load, dissipated within the first few days after loading. On day 85 after the loading, a sudden increase in settlement was observed, which subsequently stabilised almost immediately (see Fig. 23). The total horizontal stress and excess pore pressure readings measured by the spade cells also indicated a similar sudden jump at the same time. All three piezometer readings increased by 7.7 kPa indicating the water table in the foundation pit (above foundation level) rose from  $\sim 0.4$  m to  $\sim 1.2$  m (rise of  $\sim 0.8$  m). Comparing these measurements with the rainfall and evaporation data of the Bureau of Meteorology of the Australian Government (blue<sup>1</sup> shaded area in Fig. 27) indicates that the

<sup>1</sup> For interpretation of color in Fig. 27, the reader is referred to the web version of this article.

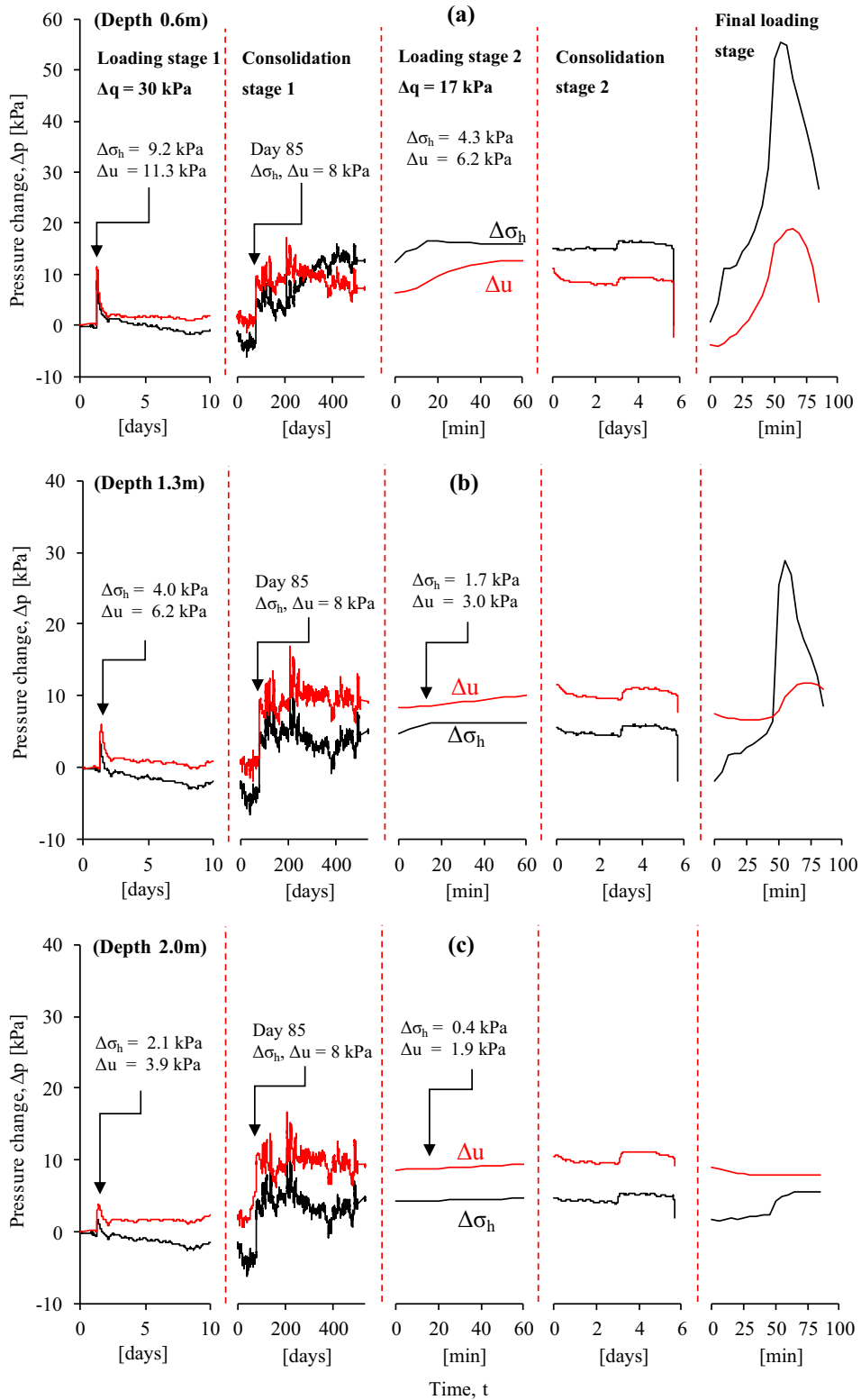


Fig. 24. Change in total horizontal pressure and pore pressure measurements from spade cells at (a) 0.6 m, (b) 1.3 m and (c) 2.0 m below foundation level; Test CU2.

Table 1  
MCC parameters of the Ballina clay in the foundation FE analyses.

Depth [m]	M [-]	$R_0$ [-]	$\kappa^*$ [-]	$\Lambda$ [-]	$\mu$
1.5–2.0	1.33	1.28	0.022	0.92	0.1
2.0–3.0	1.26	1.21			
3.0–5.0	1.22	1.12			
5.0–10	1.20	1.08			

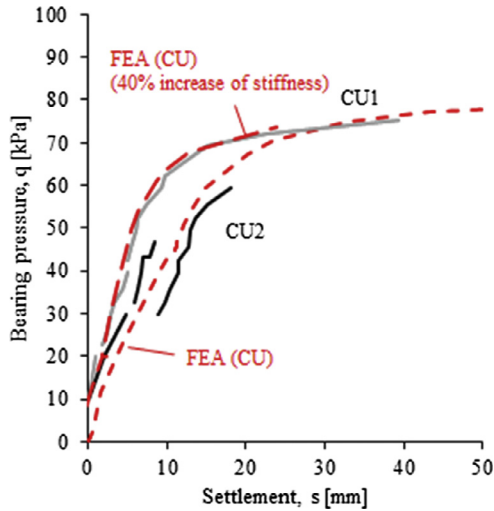


Fig. 25. Comparison between the observed CU1 and CU2 load-settlement response and the corresponding FEA.

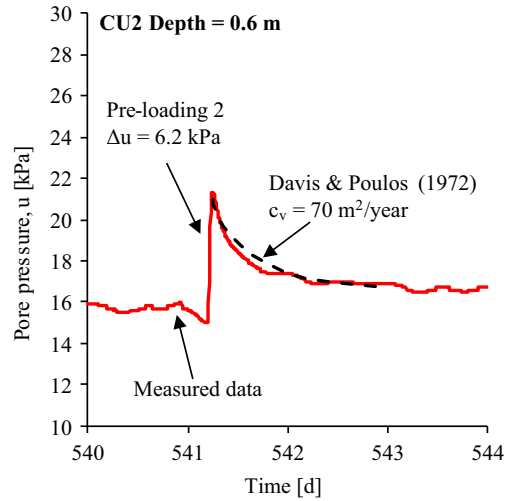


Fig. 28. Pore pressure measurements during the second loading stage and consolidation period.

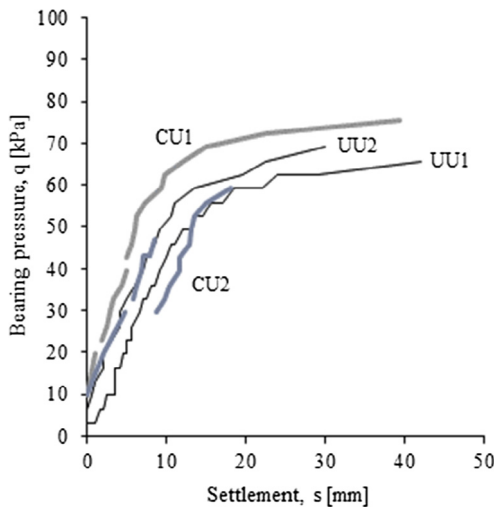


Fig. 26. Comparison between the observed undrained and consolidated undrained load-settlement response.

piezometer measurements were related to heavy rainfall event during this time that caused both foundation pits to rapidly flood.

The second loading and consolidation stage was carried out in order to facilitate interpretation of the consolidation response given the difficulty and uncertainties with the data from the first consolidation stage. A detailed picture of the pore pressure response at a depth  $z = 0.6$  m during the second consolidation stage of CU2 is shown in Fig. 28. The consolidation process, here expressed by the dissipation of the excess pore pressure and hence the increase in effective stress was analysed using a one-dimensional solution [29]. The solution is based on the simple diffusion theory but accounts for footing shape and soil anisotropy. The relationship between the vertical and horizontal coefficients of consolidation (see Fig. 4) is mostly unknown, especially for the shallow depth of interest, and therefore assumed isotropic, i.e.  $c_v/c_h = 1$ . The one-dimensional conditions for excess pore pressure dissipation were considered acceptable in this situation as the pore pressure measurements are close to the centre of the foundation. Settlement prediction, governed by excess pore pressure dissipation across the affected soil domain, will be affected by three dimensional flow and strain effects. The best fit between the mea-

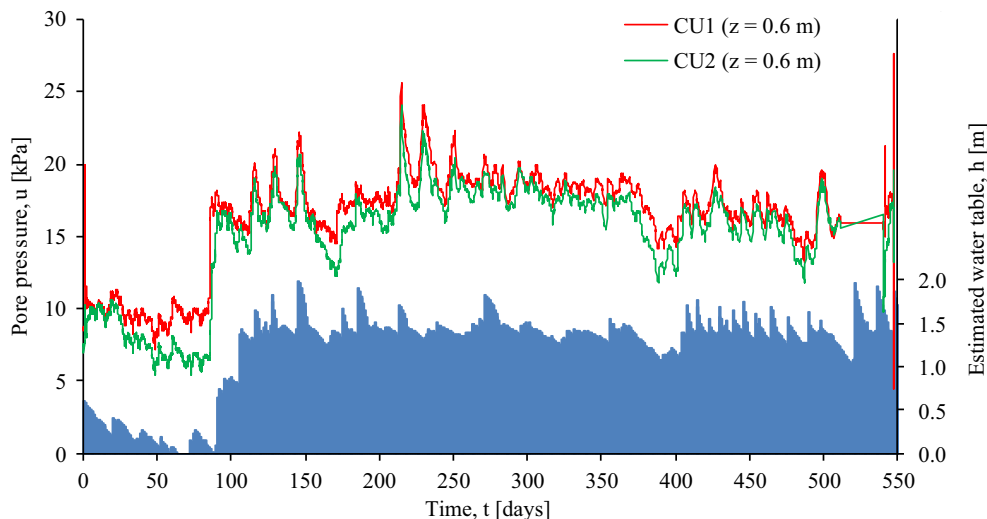


Fig. 27. Pore pressure measurements and estimated water table based on rainfall and evaporation data.

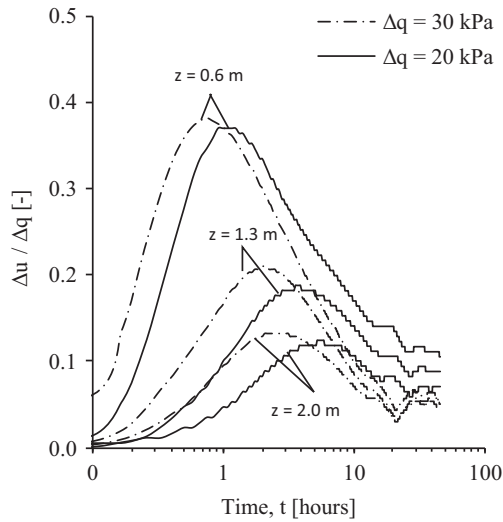


Fig. 29. Excess pore pressure normalized by applied bearing pressure  $\Delta q$ .

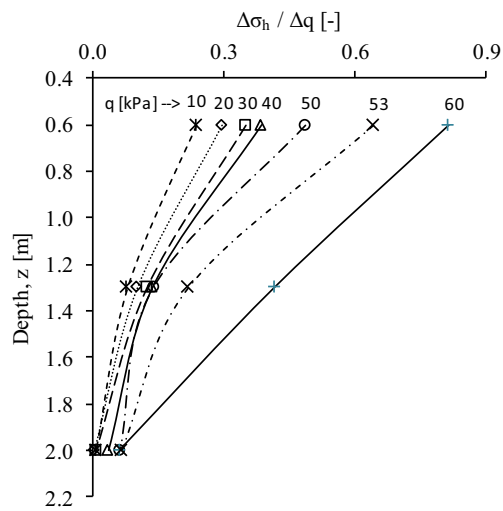


Fig. 30. Total horizontal stress normalized by applied bearing pressure  $\Delta q$ .

sured pore pressure dissipation and the approach of [29] was achieved using a  $c_v$  of  $70 \text{ m}^2/\text{year}$ . This value is consistent with the summarised results of oedometer tests on soil samples from shallow depths and the same effective stress range,  $\sigma'_v$  and the data provided in Fig. 4 [13]. However, it is noted that in situ and laboratory tests indicated a strong variation in the coefficient of consolidation,  $c_v$ , in the first few metres below ground level, ranging from  $5$  to  $150 \text{ m}^2/\text{year}$  [13] and the solution only represents an average value of  $c_v$  [29].

Fig. 29 shows the dissipation of the excess pore pressure beneath the foundation in test CU2 normalized by the applied bearing pressure against time. The normalized dissipation is shown for different changes of bearing pressure and it can be seen that the ratio is consistent with depth. At a depth of  $z = 0.6 \text{ m}$  below the foundation base the increase in pore pressure is around 38% of the applied bearing pressure. This ratio drops to 20% at  $z = 1.3 \text{ m}$  and 14% at  $z = 2.0 \text{ m}$  below the foundation base. It is also apparent from Fig. 29, that for all depths, the pore pressure response to the second pre-loading is delayed compared to the response of the first pre-loading, which may be a consequence of the consolidation process and the accompanied decrease in coefficient of consolidation.

In Fig. 30, the variation in total horizontal stress normalized by the applied load is shown against depth. It can be seen that the ratio between recorded and applied stress also increased with increasing stress level.

#### 4.2.5. Consolidated undrained bearing capacity

A more detailed picture of the load-settlement response for the final loading stage, showing the vertical movement of each corner target and the direction of the foundation tilt, is provided in Fig. 31. The consolidated undrained foundation tests failed by rotating towards a corner, similar to the UU tests as shown in Figs. 16 and 17.

The interpretation of the failure load for the CU tests followed the same procedure as for the UU tests. The maximum permissible load in test CU1 was  $70 \text{ kPa}$ ,  $\sim 15\%$  greater than in the UU tests. The failure load mobilised in CU2 was  $60 \text{ kPa}$  – identical to the failure load observed in the UU tests. The low failure load in test CU2 is assumed to be a result of load eccentricity and/or cyclic effects of rapid unloading reloading (as described above). Because of this influence on the consolidated undrained capacity in test CU2, the representative gain in bearing capacity is taken as that observed in test CU1.

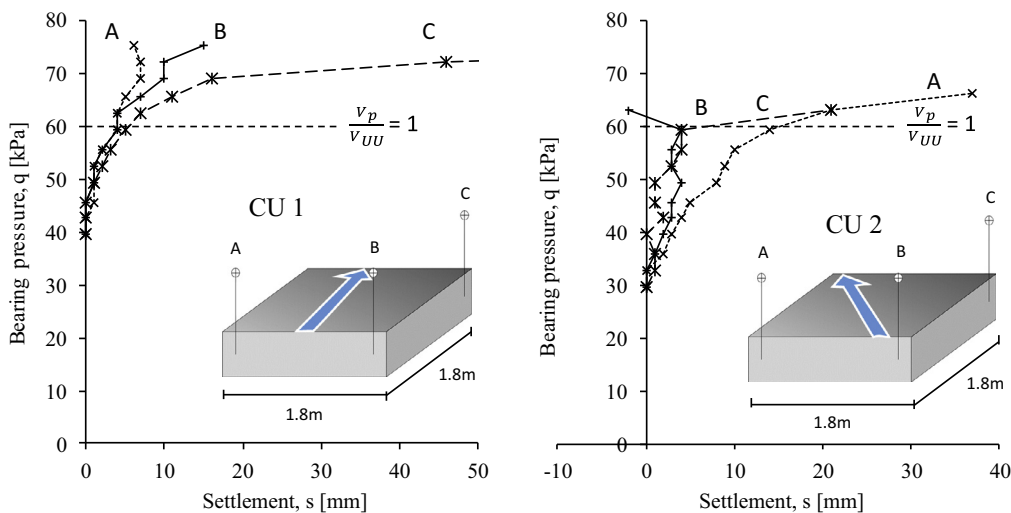


Fig. 31. Load-settlement response of the consolidated undrained foundation tests (CU1 and CU2).

Figs. 20 and 25 show the results of a FE analysis of the UU and CU tests. It can be seen, that the gain in bearing capacity due to consolidation can be well predicted using the MCC soil model and the soil parameter given in Table 1.

The gain in undrained vertical bearing capacity of a shallow foundation due to preloading and consolidation was also predicted using a theoretical framework based on critical state soil mechanics concepts [30]. The affected area of soil is treated as a 'lumped element' and traditional critical state relationships between changes in effective stress, void ratio and shear strength are adopted. The parameters used for predicting the gain in bearing capacity was taken as those used for the consolidated undrained FEA. The predicted increase in undrained capacity, given as a ratio of the consolidated undrained capacity to the immediate, unconsolidated undrained capacity,  $V_{CU}/V_{UU} = 14\%$  was in good agreement with field observations, despite the theoretical framework considering a surface foundation with a free surface surcharge. The critical state framework for predicting the consolidated undrained bearing capacity of a shallow foundation [30] is available as a free web app at [www.webappsforengineers.com](http://www.webappsforengineers.com) and provides a useful tool as a quick estimate of consolidated gains in vertical bearing capacity.

## 5. Conclusion

A programme of large-scale instrumented shallow foundation field tests investigating the undrained and consolidated undrained load-settlement response and ultimate capacity under vertical centric loading has been carried out at the Australian National Field Testing Facility (NFTF) for soft soils. Site works and activities in preparing the tests are presented along with load- and time-settlement observations to failure. The load-settlement response, ultimate capacity and failure mode of the two unconsolidated undrained tests agreed well with each other providing confidence in the construction and testing procedures and the uniformity of the site over the area of the tests. The successful consolidated undrained (CU) test indicated an increase in bearing capacity due to the preload and consolidation phase, which was well predicted by a critical state based framework. The load-settlement response and ultimate limit state of the unconsolidated undrained tests (UU) were shown to be well predicted by numerical analysis using a simple elastic perfectly plastic constitutive model. Comparison of the observed and predicted load-settlement response were the subject of an international prediction exercise, the results of which are presented in a companion paper in this special issue.

The programme of field tests presented in this paper adds to a sparse database of large-scale shallow foundation tests on soft clay on sites with extensive site characterisation. Such studies provide an essential benchmark for assessing techniques and methods for deriving stiffness and strength parameters, available constitutive models and available prediction methods for shallow foundation response. Field testing provides an invaluable and convincing means of assessing analytical and numerical methods of predicting shallow foundation response.

## Acknowledgements

This work forms part of the activities of the Centre for Offshore Foundation Systems (COFS). Established in 1997 under the Australian Research Council's Special Research Centres Program. Supported as a node of the Australian Research Council's Centre of Excellence for Geotechnical Science and Engineering. The first and second authors and the work presented in this paper are sup-

ported through ARC grant CE110001009. This support is gratefully acknowledged. The authors also extend their thanks to Dr. Cathal Colreavy and Dr. Richard Kelly who assisted with the site preparations and tests.

## References

- [1] Doherty JP, Gaone FM, Gourvenec S. Insights from a shallow foundation load-settlement prediction exercise. *Comput Geotech* 2017;93:269–79.
- [2] Jardine RJ, Lehané B, Smith PR, Gildea PA. Vertical loading experiments on rigid pad foundations at Bothkennar. *Géotechnique* 1995;45:573–97.
- [3] Lehané B, Jardine RJ. Effects of long-term pre-loading on the performance of a footing on clay. *Géotechnique* 2003;53:689–95.
- [4] Institution of Civil Engineers. Bothkennar soft clay test site: characterization and lessons learned. *Géotechnique* 1992;42:161–2.
- [5] Shields DH, Bauer GE. Determination of the modulus of deformation of a sensitive clay using laboratory and in-situ tests. In: *In Situ Measurement of Soil Properties* 1975. p. 395.
- [6] Jardine RJ, Fourie A, Maswoswe J, Burland JB. Field and laboratory measurements of soil stiffness. In: 11th ICSMFE, San Francisco. p. 511–4.
- [7] Wood DM. Yielding in soft clay at Bäckebol, Sweden. *Géotechnique* 1980;30:49–65. <http://dx.doi.org/10.1680/geot.1980.30.1.49>.
- [8] Watson GH, Crooks JHA, Williams RS, Yam CC. Performance of preloaded and stage-loaded structures on soft soils in Trinidad. *Géotechnique* 1984;34:239–57. <http://dx.doi.org/10.1680/geot.1984.34.2.239>.
- [9] Kabbaj M, Tavenas F, Leroueil S. In situ and laboratory stress-strain relationships. *Géotechnique* 1988;38:83–100. <http://dx.doi.org/10.1680/geot.1988.38.1.83>.
- [10] Doherty JP, Gourvenec S, Gaone FM, Kelly RB, Pineda JA, O'Loughlin C, et al. A novel web based application for storing, managing and sharing geotechnical data, illustrated using the National soft soil field testing facility in Ballina, Australia. *Comput Geotech* 2017;93:3–8.
- [11] Kelly RB, Sloan SW, Pineda JA, Kourtezis G, Huang J. Outcomes of the Newcastle symposium for the prediction of embankment behaviour on soft soil. *Comput Geotech* 2017;93:9–41.
- [12] Pineda J, McConnell A, Kelly R. Performance of an innovative direct-push piston sampler in soft clay. In: *Proc CPT'14*; 2014.
- [13] Pineda JA, Suwal LP, Kelly RB, Bates L, Sloan SW. Characterisation of Ballina clay. *Géotechnique* 2016;66:556–77.
- [14] Kelly R, Pineda J, Mayne P. In-situ and laboratory testing of soft clays. *Aust Geomech J* 2013;48:61–72.
- [15] Kelly RB, O'Loughlin CD, Bates L, Gourvenec S, Colreavy C, White DJ, et al. In situ testing at the National Soft Soil Field Testing Facility, Ballina, New South Wales. *Aust Geomech* 2014;50(4):13–26.
- [16] Colreavy C, O'Loughlin CD, Randolph MF. Estimating consolidation parameters from field piezoball tests. *Géotechnique* 2016;66:333–43. <http://dx.doi.org/10.1680/jgeot.15.p.10>.
- [17] Gaone FM, Doherty JP, Gourvenec S. Self-boring pressuremeter tests at the National Field Testing Facility, Ballina NSW. In: 5th international conference on geotechnical and geophysical site characterization. p. 761–6.
- [18] Gaone FM, Doherty JP, Gourvenec S. An optimisation strategy for evaluating modified Cam clay parameters using self-boring pressuremeter test data. [submitted for publication].
- [19] Small A. Vibrating wire pressure cell user manual 2005; Soil Instruments:1–8.
- [20] Houlby G, Martin C. Undrained bearing capacity factors for conical footings on clay. *Géotechnique* 2003.
- [21] Gourvenec SM, Mana DSK. Undrained vertical bearing capacity factors for shallow foundations. *Geotech Lett* 2011;1:101–8. <http://dx.doi.org/10.1680/geolett.11.00026>.
- [22] Becker DE, Jefferies MG, Crooks J, Been K. Geology, characterization and properties of Beaufort Sea Clays. *Charact Eng Prop Nat Soils, Tan, Phoon, Hight Leroueil* 2006:1855–91.
- [23] Reeves GM, Sims I, Cripps JC. Clay materials used in construction; 2006.
- [24] Jefferies MG, Crooks JHA, Becker DE, Hill PR. Independence of geostatic stress from overconsolidation in some Beaufort Sea clays. *Can Geotech J* 1987;24:342–56.
- [25] Silvestri V. Assessment of self-boring pressuremeter tests in sensitive clay. *Can Geotech J* 2003;40:365–87.
- [26] Jaky J. The coefficient of earth pressure at rest. *J Soc Hungarian Archit Eng* 1944;78:355–8.
- [27] Robertson PK. Soil classification using the cone penetration test. *Can Geotech J* 1990;27:151–8.
- [28] Tedd P, Powell J, Charles J, Uglow IM. In situ measurements of earth pressures using push-in spade-shaped pressure cells—10 years' experience. In: *Proc. geotech. instrum. pract. purp. perform. interpret*. Telford, London. p. 701–16.
- [29] Davis EH, Poulos HG. Rate of settlement under two-and three-dimensional conditions. *Géotechnique* 1972;22:95–114.
- [30] Gourvenec SM, Vulpe C, Murthy TG. A method for predicting the consolidated undrained bearing capacity of shallow foundations. *Géotechnique* 2014;64:215–25. <http://dx.doi.org/10.1680/geot.13.p.101>.